Structure–Function Relations in an Elastase-Induced Mouse Model of Emphysema

Hiroshi Hamakawa[1], Erzsébet Bartolák-Suki[1,2], Harikrishnan Parameswaran[1], Arnab Majumdar[1], Kenneth R. Lutchen[1], and Béla Suki[1]

[1]Department of Biomedical Engineering, Boston University, Boston; and [2]Cellutraf Scientific Inc., Boston, Massachusetts

Emphysema is a progressive disease characterized by the destruction of peripheral airspaces and subsequent decline in lung function. However, the relation between structure and function during disease progression is not well understood. The objective of this study was to assess the time course of the structural, mechanical, and remodeling properties of the lung in mice after elastolytic injury. At 2, 7, and 21 days after treatment with porcine pancreatic elastase, respiratory impedance, the constituents of lung extracellular matrix, and histological sections of the lung were evaluated. In the control group, no changes were observed in the structural or functional properties, whereas, in the treatment group, the respiratory compliance and its variability significantly increased by Day 21 ($P < 0.001$), and the difference in parameters decreased with increasing positive end-expiratory pressure. The heterogeneity of airspace structure gradually increased over time. Conversely, the relative amounts of elastin and type I collagen exhibited a peak ($P < 0.01$) at Day 2, but returned to baseline levels by Day 21. Structure–function relations manifested themselves in strong correlations between compliance parameters and both mean size and heterogeneity of airspace structure ($r^2 > 0.9$). Similar relations were also obtained in a network model of the parenchyma in which destruction was based on the notion that mechanical forces contribute to alveolar wall rupture. We conclude that, in a mouse model of emphysema, progressive decline in lung function is sensitive to the development of airspace heterogeneity governed by local, mechanical, force-induced failure of remodeled collagen.

Keywords: lung compliance; morphology; elastin; collagen; network model

Emphysema is characterized by air space enlargement, accompanied by destruction of parenchymal structure (1), and, being a component of chronic obstructive pulmonary disease (COPD), is a major cause of chronic morbidity and mortality worldwide (2). Although lung transplantation and lung volume reduction are possible therapies, there is no cure for patients with end-stage emphysema (3).

The most accepted hypothesis of the pathogenesis of emphysema is an imbalance between elastase and antielastase activity (4) extended to include other proteases (5). Peripheral airway inflammation (6), oxidative stress (7), and apoptosis (8) are also thought to be involved in the pathogenesis. Some of these mechanisms may interact, leading to remodeling of the extracellular matrix (ECM) (9). While the exact mechanisms of pathogenesis are not fully understood, it is even less clear how the disease progresses.

(*Received in original form November 18, 2010 and in final form December 20, 2010*)

This work was supported by National Institutes of Health grant HL090757.

Correspondence and requests for reprints should be addressed to Bela Suki, Ph.D., Department of Biomedical Engineering, Boston University, Boston, MA 02215. E-mail: bsuki@bu.edu

This article has an online supplement, which is accessible from this issue's table of contents at www.atsjournals.org

Am J Respir Cell Mol Biol Vol 45. pp 517–524, 2011
Originally Published in Press as DOI: 10.1165/rcmb.2010-0473OC on December 17, 2010
Internet address: www.atsjournals.org

CLINICAL RELEVANCE

Both the separate structural and functional properties of the emphysematous lung have been well studied. However, the relation between them is not well understood. Functional properties of the emphysematous lung are most sensitive to the presence of structural heterogeneity that increases during progression due to the interaction between enzymatic degradation and mechanical forces.

In clinical practice, emphysema progression is characterized by a decline in lung function (10), directly affecting quality of life, or an increase in low attenuation area on lung computed tomography images, indicating tissue destruction (11). However, there is little correlation between indexes derived from computed tomography images and spirometric lung function (11, 12). Recently, Bates and colleagues (13) showed that lung function is relatively insensitive to the amount of tissue loss in the beginning of the destruction process. They demonstrated that lung compliance could stay relatively normal during the early phase of the disease until microscopic alterations reach a critical level, beyond which a rapid decline in function occurs. If lung function is decoupled from the amount of tissue loss, the question arises whether it is the ECM composition, ECM organization within the alveolar wall, or some feature of the alveolar wall network that determines lung function decline. Furthermore, it is equally unclear whether there is a specific mechanism that drives changes in structure that also influences function. Suki and colleagues (14) proposed that mechanical forces in the emphysematous lung contribute to the progressive nature of the disease by rupturing the remodeled alveolar walls, thus reducing tissue stiffness. They also suggested that for this mechanism to work, the weakening of collagen, a key load-bearing ECM molecule, is necessary.

In this study, we hypothesized that functional changes in emphysema are related to both the extent of collagen remodeling and specific localized alterations in alveolar airspace structure. To test this hypothesis, we tracked the remodeling of collagen and elastin, the detailed alveolar structure, and lung function in mice during 3 weeks after elastolytic injury. The results were interpreted using a network model of the parenchyma.

MATERIALS AND METHODS

Animal Preparation

Six groups of C57BL/6 mice were used. Procedures were approved by the Animal Care and Use Committee of Boston University (Boston, MA). Mice were treated with oropharyngeal instillation of either 0.25 IU of porcine pancreatic elastase (PPE) ($n = 18$) or phosphate-buffered saline (saline control) ($n = 18$). Animals were killed at 2, 7, and 21 days after treatment.

Respiratory Mechanics

Mice were anesthetized, tracheostomized, and ventilated. Respiratory impedance was measured at five positive end-expiratory pressure (PEEP) levels using forced oscillations (15). A model including a heterogeneous distribution of tissue elastance (16) was fit to the data, providing estimates of airway resistance (R_{aw}), hysteresivity, a mean tissue compliance (C_{mean}), and a minimum (C_{min}) and a maximum compliance (C_{max}). The model-based functional heterogeneity of the parenchyma was characterized by the SD of C (SD_C) calculated from C_{min} and C_{max} (*see* details in the online supplement).

Tissue Processing

Lungs were inflated with formalin at an airway pressure of 30 cm H_2O. The mediastinal lobes were embedded in paraffin, and 7-μm sections were obtained. The lung was homogenized in the presence of protease inhibitors, and the supernatant stored. In four additional controls and four PPE-treated mice, mechanics were measured at a PEEP of 3 cm H_2O 21 days after treatment, and the lungs were fixed and processed for morphometry.

Morphometry

Lung sections were stained with hematoxylin and eosin. Randomly selected sections were photographed. The digitized images were automatically segmented, and the area of airspaces was measured. The equivalent diameter (D) of airspaces was determined and the mean equivalent diameter (D_{eq}) was calculated from a minimum of 500 values per mouse (limited to $D > 5$ μm). The area-weighted mean equivalent diameter (D_2) was also computed (17).

Collagen and Elastin Visualization on Histological Sections

To visualize the total amounts of collagen and elastin, the well established methods of Masson's trichrome (adapted from http://stainsfile.info) and Miller's elastic stainings (adapted from http://www.ihcworld.com/) were used, respectively. Lung sections were randomly selected.

Western Blot

The samples were normalized to equal volume, separated by gel electrophoresis, and transferred to polyvinylidene fluoride membrane. Rabbit polyclonal anti–collagen I, mouse monoclonal anti–collagen III, goat polyclonal anti-elastin, and mouse monoclonal anti–β-actin antibodies were used. The immune complexes were detected with a chemiluminescence kit and quantified by computerized densitometry.

Network Modeling

A two-dimensional rectangular network of linear elastic springs was used. A uniform negative pressure around the network mimics pleural pressure generating tensile forces on the springs. Emphysema progression was simulated in three ways at subsequent iterations: (*1*) springs were uniformly weakened; (*2*) springs were randomly eliminated; and (*3*) springs carrying high force were eliminated based on previous findings (18). The compliance, C, of the network was calculated, and the iterations were repeated until C increased by 2.

Statistical Analysis

Unpaired t test, one-way ANOVA, and two-way repeated measures ANOVA were used to evaluate differences among different time points and PEEP levels. The Kolmogrov-Smirnoff test was used to compare the distributions of D corresponding to different animals within a given treatment group. Statistical significance was accepted for a P value less than 0.05.

RESULTS

Both the control and the elastase treatment groups tolerated the oropharyngeal aspiration method well. The mortality rate from the liquid aspiration and the elastolytic injury was zero. There was no difference in weight between the age-matched control and treatment groups.

Dynamic Mechanical Properties

Although all mechanical parameters were estimated, in this study we only focus on R_{aw} and the C_{mean}, C_{min}, C_{max}. As a measure of variability of regional compliance, we also calculated the SD_C of C_{mean} for each mouse. The time course of these mechanical parameters obtained at a PEEP of 3 cm H_2O is shown in Figure 1. One-way ANOVA showed that none of these parameters changed over the 21 days in the control group. The R_{aw} decreased slightly, but not statistically significantly, with time in the treatment group, becoming significantly lower ($P < 0.05$) than that in the control group only at 21 days (Figure 1A). In the treatment group, the compliance parameters showed a gradual and statistically significant increase with time, reaching higher values than in the control group ($P < 0.001$) by 21 days (Figures 1B–1D).The C_{mean} mirrored both C_{max}, a parameter that reflects the softest region, and C_{min}, which is related to the stiffest region. The variability of compliance SD_C increased by approximately 50%, becoming significantly higher than that in the control group by 21 days (Figure 1D).

The PEEP dependence of these parameters is presented only at Day 21 (Figure 2). Two-way repeated measure ANOVA showed that C_{mean} did not depend on PEEP (Figure 2C), but the other parameters significantly depended on PEEP ($P < 0.0001$) (Figures 2A, 2B, and 2D), and treatment had a strong and significant effect ($P < 0.0001$) on these parameters. The pattern of PEEP dependence was similar for C_{max} and SD_C, and these parameters also showed a strong interaction between treatment and PEEP ($P < 0.0001$). Interestingly, for C_{max}, C_{mean}, and SD_C, the difference between groups gradually decreased, with no difference at the higher PEEP levels (Figures 2B–2D).

Lung Tissue Structure

Figure 3 shows collagen (Figures 3A–3D) and elastin (Figures 3E–3H) stained representative histological sections from the control and the treatment groups at 2 and 21 days after treatment. The heterogeneous structure suggesting significant destruction of alveoli can be readily seen in the images from the treatment group at Day 21 (Figures 3D and 3I; *see* also Figure E1 in the online supplement). Because no difference was found between the D_{eq} corresponding to different animals within any group at any time point, data from different mice were combined for comparison between the two treatment groups (Table 1). The D_{eq} did not depend on treatment. However, the distribution of diameters was very different ($P < 0.001$) between the control and the treatment groups for all time points. To estimate the variance of D_2, the values of D in each group were randomly divided into five subgroups, which allowed the calculation of the mean as well as the SD of D_2, and, hence, statistical comparison between groups. The D_2 between the saline and PPE treatment groups was different at all time points ($P < 0.01$). Although the absolute volume of the right lobes in the four additional control and 21-day–treated mice were different, with values of 0.62 (±0.05) ml and 0.81 (±0.06) ml, respectively ($P < 0.005$), morphometry, and physiology in these animals were similar to those in the main groups.

The images in Figures 3A–3D show all collagen subtypes in blue, and every other structural component in reddish color. The elastin staining in Figures 3E–3H shows similar structure, with black representing elastin. At Day 21, missing septal walls, suggestive of failure, can be seen in the PPE group (green arrow in Figure 3H). Interestingly, thickened and short septal wall remnants were often observable, with both collagen and elastin bundles at the tip (black arrows in Figures 3D and 3H).

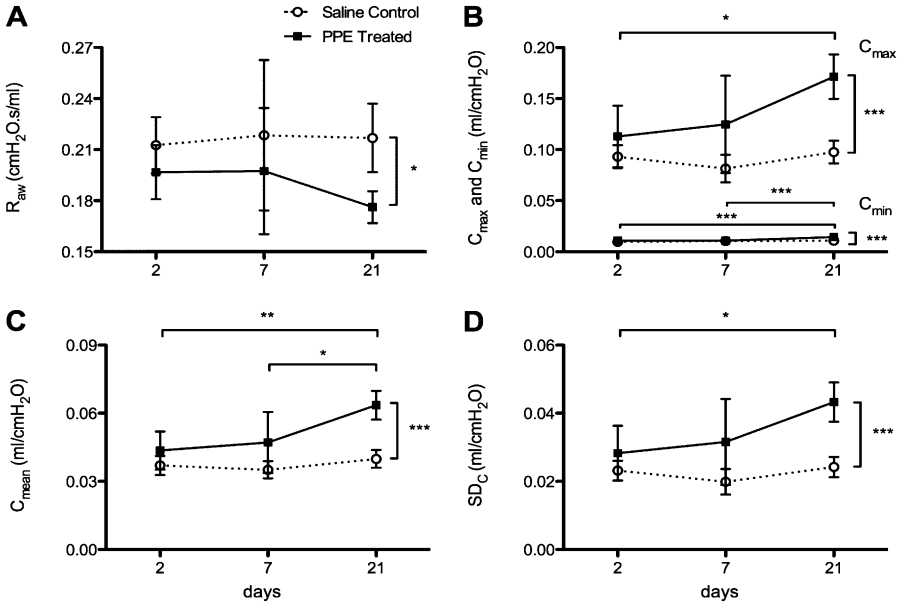

Figure 1. Time course of the mechanical parameters. (*A*) airway resistance (R_{aw}), (*B*), minimum (C_{min}) and maximum compliances (C_{max}), (*C*) mean compliance (C_{mean}), and (*D*) SD of compliance (SD_C) in saline control and porcine pancreatic elastase (PPE)–treated mice. *Stars* denote significant pair-wise difference between two groups. *Horizontal brackets* denote difference between groups at different times, and *vertical brackets* denote difference between treatment at Day 21. *$P < 0.05$, **$P < 0.01$, and ***$P < 0.001$.

ECM Composition

Representative Western blots for types I and III collagen and elastin, together with β-actin, are shown in Figure 4. In the control mice, there was no difference in the relative amounts of elastin, collagen I and III, and the collagen III:collagen I ratio in the soluble part of the ECM at any time point (Figure 5). After PPE treatment, the relative amounts of elastin and collagen I exhibited a distinct peak ($P < 0.01$) at Day 2 (Figures 5A and 5B), but there was no change in the level of type III collagen (Figure 5C). However, the collagen III:collagen I ratio showed interesting dynamics: at Day 2, it was lower than that of the control group ($P < 0.01$), but increased and reached the range of the control group by Day 21 (Figure 5D).

Structure–Function Relations

To understand better the relation between structure and function, the compliance parameters and structural parameters are correlated in Figure 6. There was a strong association between C_{mean} and D_{eq}, and an even stronger relation between C_{mean} and D_2, with r^2 values of 0.675 ($P < 0.01$) and 0.933 ($P < 0.001$), respectively (Figure 6A). There was also a strong correlation between structural and functional variabilities: the r^2 between D_2 and SD_C was 0.881 ($P < 0.01$, Figure 6B). There were no appreciable correlations between any of the ECM constituents in Figure 5 and the functional parameters.

Model Simulations

To interpret these structure–function relations, we used a network model of the parenchyma with three types of mechanisms (uniform softening, random cutting, and strain-based cutting) to simulate the increase in compliance observed in the experimental data. After proper normalization described in the online supplement, the model simulations can be compared with the experimental data (Figure 7). It can be seen that each of these mechanisms produces an approximately linear relation between the normalized compliance and the normalized D_2 of the network during simulated disease progression, but the slopes of these relations are distinct. The data corresponding to the

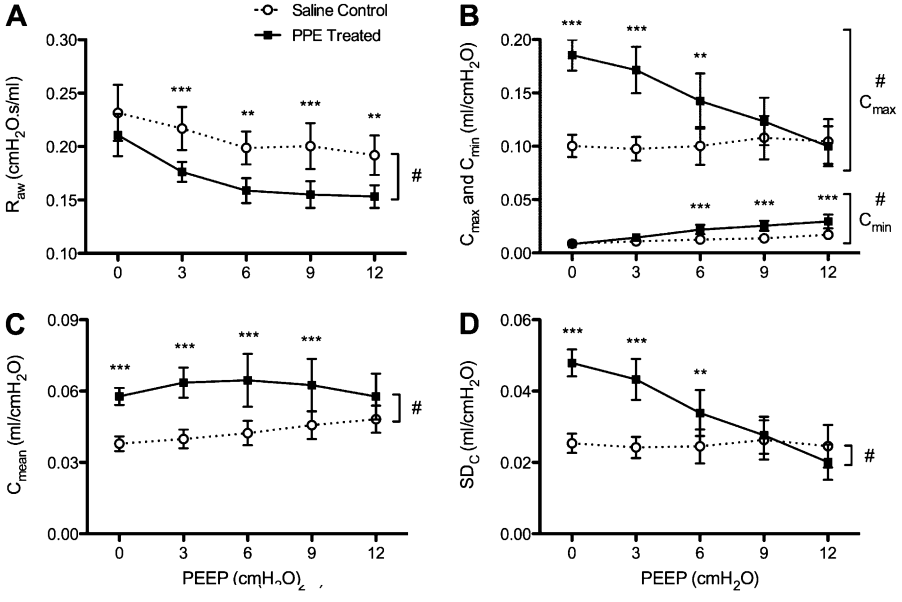

Figure 2. Positive end-expiratory pressure (PEEP) dependence of the mechanical parameters. (*A*) R_{aw}, (*B*) C_{min} and C_{max}, (C) C_{mean}, (*D*) SD_C in saline control and PPE-treated mice. The overall group differences: #$P < 0.0001$. *Asterisks* denote significant pair-wise difference between groups at the same PEEP. *$P < 0.05$, **$P < 0.01$ and ***$P < 0.001$.

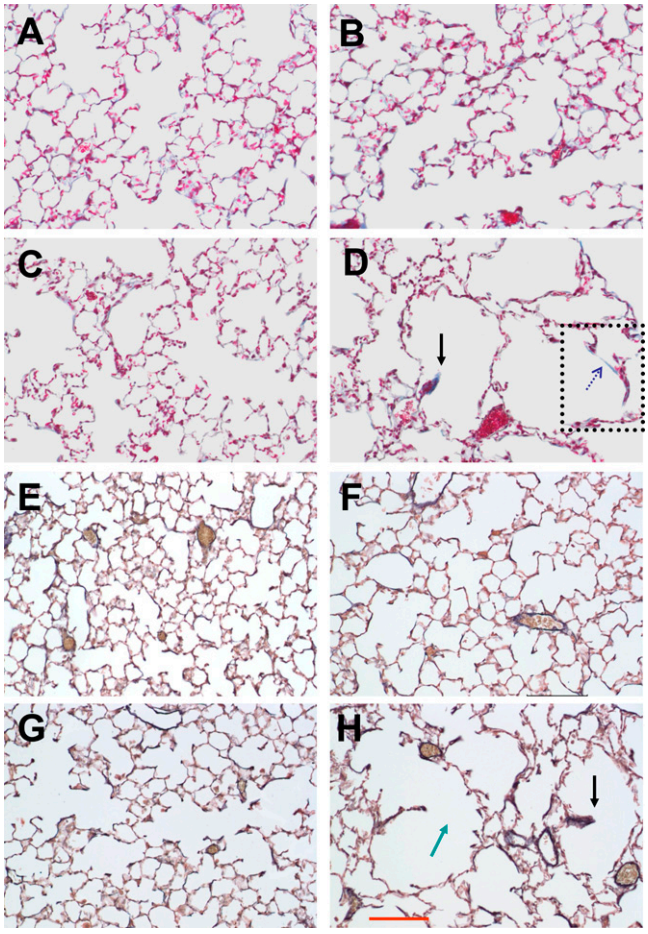

Figure 3. Examples of collagen- (*A–D*) and elastin (*E–I*)-stained images of the lung parenchyma in saline control lungs at Day 2 (*A* and *E*) and Day 21 (*B* and *G*) and in PPE-treated lungs at Day 2 (*C* and *F*) and Day 21 (*D* and *H*). The *green arrow* locates a potential site of rupture, and the *black arrows* represent thickened, retracted septal wall tissue. The region surrounded by the *dotted rectangle* is enlarged in the online supplement. The *dotted blue arrow* shows a stretched alveolar wall containing only collagen. The *red scale bar* in (*H*) represents 100 μm.

strain-based destruction best approximates the experimental data. However, although C_{mean} doubles, the rate of increase of D_2 is still larger in the experimental data than in the simulations. Also note that these simulations do not represent best fits.

DISCUSSION

Many studies using mouse models of pulmonary emphysema reported changes in the functional mechanical (16, 19–21), structural (16, 22–25), or biochemical (9, 20, 22, 25–29) properties of the lung. The purpose of the present study was to shed light on the relation among these properties, namely, on structure–function relations. Specifically, we sought to determine how the functional decline is related to alveolar airspace structure and the biochemical composition of the lung parenchyma during the progression of an elastase-induced mouse model of emphysema. Lung function was characterized by the detailed mechanical properties of the respiratory system, alveolar structure was analyzed using advanced morphometric techniques, and biochemical composition was assessed by determining the soluble components of the main load-bearing ECM proteins, collagen types I and III and elastin. Besides the usual observations that lung compliance increases and the airspace structure is destroyed, our main findings are: (*1*) changes in lung compliance were decoupled from changes in the biochemical properties of the tissue; (*2*) lung compliance correlated best with the variability of the peripheral airspace structure; (*3*) model-based variability in lung compliance also correlated with the variability of airspace sizes; and (*4*) the observed structure–function relations are best described by a model in which tissue deterioration is associated with mechanical forces.

The elastase-induced emphysema model has several limitations. First, elastase produces localized injury, and the subsequent immune response and remodeling processes in the mouse are different from those in humans. Second, relative to the life span of the mouse, the time course of the development of emphysema in mice is much faster than that in humans. Third, the chest wall plays a different role in mice than in humans, because the chest wall tissues are very soft in the former (16, 30). The latter is an advantage, however, as it allows us to use respiratory mechanics as a surrogate for lung mechanics, which obviates the need for the unphysiological open-chest condition. Another advantage is that the fast development of structural destruction allows us to investigate the detailed time course of the progression. Furthermore, the elastase–injury model has been shown to produce airspace enlargement and increases in lung volumes and compliance similar to those in human patients (31). Thus, this model should be adequate for a first-order evaluation of structure–function relations during disease progression.

After elastolytic injury, R_{aw} decreased relative to control (Figure 1A) and decreased with increasing PEEP (Figure 2A). These functional changes were similar to those observed in the tight-skin mice (32), which spontaneously develop lung structure similar to pulmonary emphysema early in life (33). Sly and colleagues (19) measured respiratory mechanics in the surfactant protein (SP)–D–deficient mouse, which develops emphysema with age, and found that R_{aw} was lower than in wild-type mice and decreased with increasing lung volume. Lundblad and colleagues (21) observed a similar decreasing pattern of R_{aw} with increasing PEEP in surfactant protein C/TNF-α–transgenic mice, which have severe emphysematous lesions. Thus, the

TABLE 1. LUNG MORPHOMETRY IN PORCINE PANCREATIC ELASTASE–TREATED AND SALINE CONTROL MICE

	Saline Control		PPE Treated		Significance		
Days	D_{eq} ± SD (μm)	D_2 ± SD (μm)	D_{eq} ± SD (μm)	D_2 ± SD (μm)	D_{eq}	K-S Test	D_2
2	27.8 ± 13.5	44.3 ± 2.9	30.2 ± 16.5	54.6 ± 4.7	NS	$P < 0.001$	$P < 0.01$
7	27.6 ± 13.2	43.4 ± 2.8	31.3 ± 16.8	57.2 ± 5.6	NS	$P < 0.001$	$P < 0.01$
21	28.1 ± 17.0	57.2 ± 5.0	34.0 ± 26.3	109.7 ± 32.8	NS	$P < 0.001$	$P < 0.01$

Definition of abbreviations: D_2, area-weighted mean equivalent diameter; D_{eq}, mean equivalent diameter; PPE, porcine pancreatic elastase; K-S, Kolmogorov-Smirnoff test.

The SD of D_{eq} represents the variability of the equivalent diameter, whereas the SD of D_2 represents the error of regional D_2.

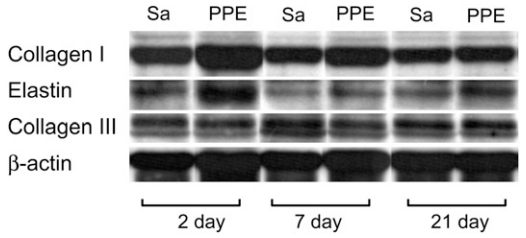

Figure 4. Example Western blots for collagen types I and III and elastin in saline control (Sa) and PPE-treated lungs at various time points. The molecular weights are between 95 and 130 kD for collagen I, around 70 kD for collagen III, and between 60 and 65 kD for elastin. Each Western blot had its own beta-actin loading control; the bottom row shows one example.

general trends of the time and PEEP dependence of the physiologic parameters are not specific to the elastase injury. It is likely that the lower R_{aw} in this study was a consequence of increased lung volumes after treatment. Hantos and colleagues (31) recently reported that, in a virtually identical elastase-induced emphysema model, thoracic gas volume in mice increased by 50% and R_{aw} was higher in the treatment group when the comparison was made at similar absolute lung volumes. In our complementary experimental groups, there was a 31% increase in absolute lung volume at 30 cm H_2O fixation pressure by 21 days. Hence, at the same PEEP, absolute lung volume is higher in the treated lung, and, consequently, airways are pulled open more, resulting in a lower R_{aw}.

Respiratory system compliance, C_{mean}, as a surrogate of lung tissue compliance, was estimated using a heterogeneous model of the lung (16) and increased with time (Figure 1C). The increase in compliance or decrease in elastance is a hallmark feature of emphysema (16, 20–22, 25, 31, 34–38), and is a consequence of parenchymal tissue destruction. By incorporating a distribution of compliances in our heterogeneous impedance model, we also obtained estimates of the minimum and maximum regional compliance values, C_{min} and C_{max}, respectively, in the lung. The C_{max} represents the compliance of a region with the most severe destruction, such as the big defect holes in Figures 3D and 3I, where the number of alveolar walls per unit area is the smallest. Interestingly, C_{mean} followed a similar pattern as C_{max}. On the other hand, C_{min} is related to the stiffest region of the lung. The C_{min} showed a small but statistically significant increase in the treatment groups compared with controls. This implies that no region in the treated lung reached the smallest compliance corresponding to the normal lung. From C_{min} and C_{max}, we also calculated the variability of regional compliance characterized by SD_C, which increased significantly in the treatment groups by Day 21. A striking functional change was seen in the treatment at Day 21 causing a significant qualitative change in the PEEP dependence of C_{max} and SD_C (Figure 2). Although the reason for this is not entirely clear, we speculate that it was caused by the recruitment of the soft and collapsed regions at low PEEPs, followed by the recruitment of stiff collagen in the more intact regions causing an overall rapid stiffening of the whole lung with increasing PEEP.

Despite the functional decline and the increase in absolute lung volume by Day 21, there was no significant enlargement in alveolar airspace size, as characterized by D_{eq} at any time point (Table 1). The lack of an increase in D_{eq} is due to the presence of spatial heterogeneities, with a large variability of air space sizes, which would be similarly reflected in other average morphometric measures, such as the mean linear intercept (17). However, both the distribution of D and the D_2, which is a sensitive measure of heterogeneities (17), were different in all groups at all time points. Again, these observations are not limited to the elastase model, because the tight-skin and pallid mice also showed similar increases in heterogeneities (32). Thus, the structural characterization of the lung cannot be based on mean values; instead, our data imply that a key histopathological feature of the lung during the progression of emphysema is the appearance of an increase in structural heterogeneity.

As discussed above, by Day 21, we also observed a decline in lung function, characterized by increases in C_{mean} and SD_C. Although this model-based functional heterogeneity is more representative of the asynchronous temporal distribution of

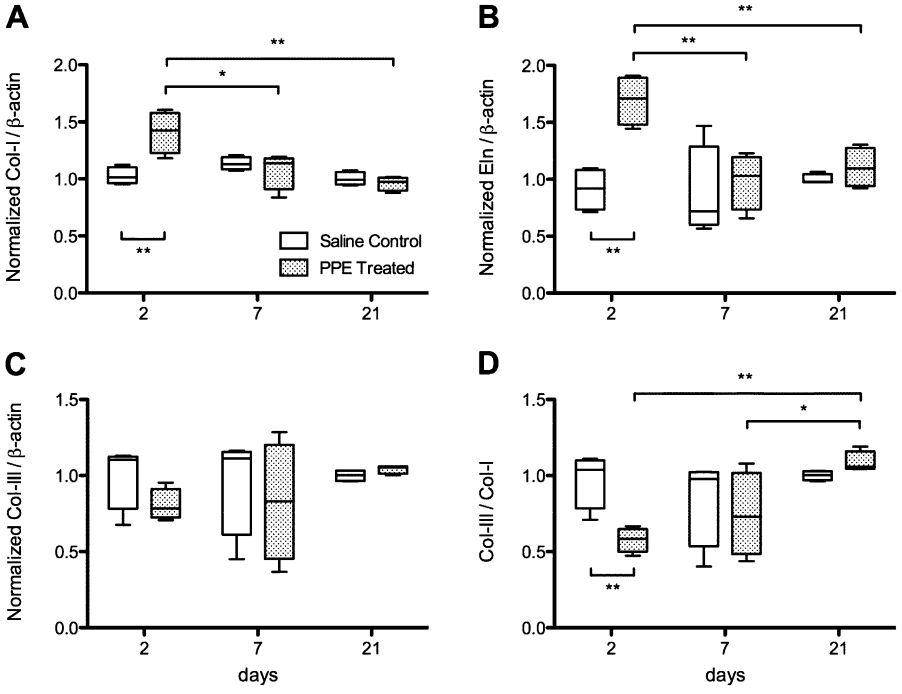

Figure 5. Time course of collagen I (*A*) and III (*C*), elastin (*B*), and the ratio of collagen III:collagen I, each normalized by their loading control, as well as normalized to unity with the mean of the saline control at Day 21. *Asterisks* denote significant differences as described in the caption to Figure 1. $*P < 0.05$ and $**P < 0.01$.

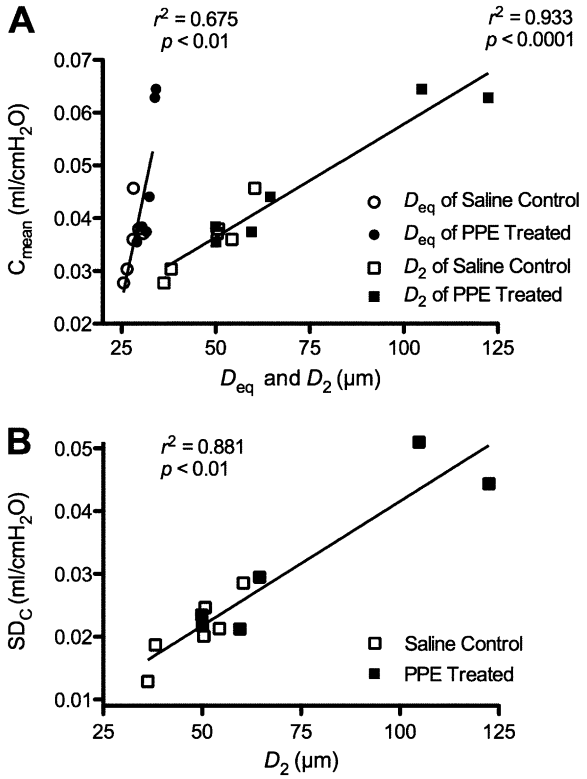

Figure 6. Structure–function relations obtained in saline control and PPE-treated mice. (*A*) C_{mean} as a function of the mean equivalent diameter (D_{eq}) or area-weighted mean equivalent diameter (D_2). (*B*) SD_C as a function of D_2.

ventilation during breathing, one might also expect a relation between the structural alterations and the functional decline. Indeed, when examined on an individual basis, we found a reasonable correlation between C_{mean} and D_{eq}, and a strong correlation between C_{mean} and D_2 (Figure 6A), a main result of this study. The former might be expected on the basis that an increase in airspace size is equivalent to a decrease in alveolar walls per unit volume, and hence a decrease in stiffness or increase in compliance. The latter relation was, however, much stronger (r^2=0.933), indicating that an increase in compliance is much more related to an increase in structural heterogeneity than to mean size. In other words, our experimental results suggest that producing a few large defect holes has a much greater effect on function than uniformly weakening the alveolar walls. This is in excellent agreement with the structure–function relation predicted by our network model (Figure 7). Figure 6B also shows a strong correlation (r^2=0.881) between the model-based estimate of functional heterogeneity, SD_C, and the structural heterogeneity, D_2. It is thus plausible to conclude that the formation of large defect holes produces structural heterogeneity, broadening the distribution of regional tissue compliance, which, in turn, results in a more heterogeneous distribution of dynamic lung compliance and, hence, ventilation distribution. The question is whether we can identify an underlying biochemical and/or remodeling process that would account for the structural heterogeneity.

Regional tissue compliance is a function of the local tissue density (i.e., the number of alveolar walls per unit volume) and the average elasticity of the alveolar wall tissue. Because the elasticity of the tissue should be related to the amount of elastin and collagen in the walls, we chose to track the expression of the main load-bearing elements of the ECM, collagen I and III and

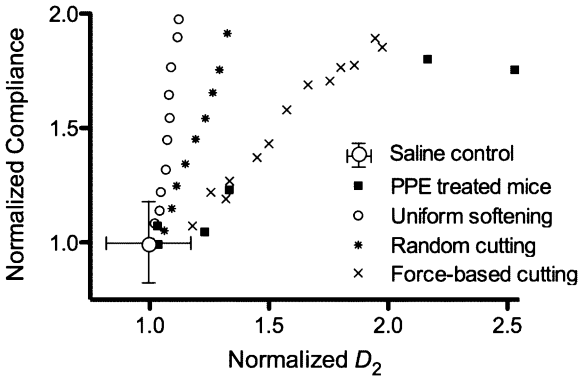

Figure 7. Comparison of structure–function relation from the network model and experiments. Experimental data were normalized with the mean value of C_{mean} and D_2 of control mice. Each *black square* corresponds to data from a single mouse. The *symbols* corresponding to the various model cases represent model outputs normalized by the output of the baseline model.

elastin. Control levels after saline treatment did not change throughout the 21 days. Compared with time 0, collagen I and elastin peaked at Day 2 after elastase exposure, but this acute ECM remodeling returned to normal by Day 21 (Figures 5A and 5B, respectively). These results are consistent with those reported by Lucey and colleagues (29). In addition, during the time course, the ratio of collagen III to collagen I first decreased in the early phase, then gradually returned to the same level as in the control group (Figure 5D). A similar decrease in collagen III:collagen I ratio was also observed in the matrix metalloproteinase (MMP)-1 transgenic adult mouse model of emphysema (28). Surprisingly, however, we found no correlations between these remodeling events and the functional parameters. The highest correlation coefficient was only 0.31 between collagen I and C_{mean}.

One potential reason for the lack of correlations could be the contribution of surface tension to recoil (39). To test this possibility, we performed complementary experiments on samples to determine the levels of SP-B, the most important protein component of surfactant regulating surface tension. We found no difference between SP-B levels in the saline and PPE groups at Days 7 and 21 (*see* the online supplement). Because, in the treated lungs, the same amount of SP-B was distributed over a smaller total surface area, but in regions with larger radius of curvature, the recoil pressure due to surfactant (assuming that all other protein and lipid concentrations were also the same) would be less in the PPE-treated lungs. These results are in agreement with the recent findings of Mouded and colleagues (40) that, in PPE-treated mice, surface tension is normal.

Another possibility for the lack of correlations between biochemistry and function is that we investigated only the soluble components of the ECM. Mature collagen and elastin fibers are stabilized by strong cross-links, which make the fibers insoluble in saline (41), and, hence, such fibers cannot be detected through Western blots. In a previous study, we reported that the total collagen, including both types I and III, increased by approximately 45% at 21 days after elastase treatment in mice (20). Therefore, it is possible that the total collagen would correlate with the increase in C_{mean}. However, this remains highly paradoxical, as one would expect that any increase in collagen content should decrease lung compliance, as in fibrosis. One possibility is that collagen fiber assembly and/or cross-linking is abnormal during the remodeling process. Indeed, abnormal ECM remodeling has been reported in humans (42). Such abnormal repair can produce weak collagen

prone to failure (18), which, in turn, plays a role in the macroscopic weakening of the tissue with increased C_{mean}, despite the increase in total collagen content.

Our previous results revealed that, despite the 45% increase in total collagen content, the failure stress of the lung tissue decreased by roughly 40% (20). Thus, instead of the newly synthesized or the total amount of collagen, it is more likely that the local organization of collagen into fibers and their spatial distribution are the primary determinants of the mechanical strength and the physiologic function of the parenchyma in the disease state. Figures 3D and 3H show regions of thickened septal walls (black arrows), which contained both collagen and elastin. These structures are likely a result of recent septal wall ruptures. When a wall under tension fails, the tissue retracts and, because of conservation of mass, it becomes thicker. To understand better the actual process of failure, let us examine the dotted rectangle in Figure 3D (a magnified version is presented in the online supplement). This septal wall is under considerable tension, and it only contains collagen. Upon visual examination of hundreds of images similar to those in Figure 3, we found many retracted regions, and a few walls under tension, as in the dotted rectangle in Figure 3D. However, we found no evidence of elastin in such highly stretched thin walls. These results provide further experimental support to the notion that, ultimately, it is the failure of collagen that determines local tissue failure (18).

The simulation results showed that although a linear relation between normalized compliance and normalized D_2 exists (Figure 7), the slope of this relation was quite different among the three modes of simulated disease progression. The uniform softening failed to produce sufficient increase in D_2, suggesting that simple weakening of the alveolar walls cannot increase structural heterogeneity, consistent with experimental data. Additional simulations showed that heterogeneous softening is also unable to produce sufficient structural heterogeneity (data not shown). Although the random cutting method resulted in a larger increase in D_2, it also underestimated the experimentally observed increase in D_2. Furthermore, the random cutting method required the elimination of a large number of springs to double the compliance of the network. When springs were removed from the network based on the highest strains, the model required substantially fewer springs to be removed for a doubling of the compliance, and this process resulted in a doubling of D_2. The model still underestimates the experimentally observed 2.5-fold increase in D_2. This modest discrepancy can be due to several factors. First, the C_{mean} is derived from dynamic impedance measurements, whereas the compliance of the model is static. The compliance of the lung is frequency dependent, and the static compliance is always higher than the dynamic. Second, as Table 1 suggests, the coefficient of variation of D is approximately 30% in the control lungs. This large variability is likely a result of the presence of alveolar ducts. Even though we did not quantify the number of ducts from the images, to mimic the large coefficient of variation in control lungs, we simply used a small amount of force-based cutting in the baseline model. The mechanical properties of the ducts are different from those of the septal walls (43) and, hence, it is likely that the ducts would be differently degraded in emphysema from the septal walls. In contrast, in the network model, we did not include ducts, and the destruction process based on force was mainly limited to the area of the large initial holes. Despite these limitations, the model with force-based destruction produces a structure–function relation that is in good agreement with our experimental findings.

The above experimental and simulation results are consistent with the notion that mechanical forces present in the lung govern the destruction process, which, in turn, can also offer a mechanism for the irreversible and progressive nature of the disease. The physical rupture of an alveolar wall has two consequences: it irreversibly changes the local structure, and it influences function. Indeed, the most significant effect a microscopic event can have on macroscopic function is seen when a wall that carries a large tension fails. After the failure of a load-bearing element, the local structure rearranges itself in a manner that is consistent with elastic equilibrium, corresponding to the smallest potential energy of the network. The difference in elastic energy of the network before and after failure corresponds to a decrease in elastic recoil and an increase in compliance. At the same time, the rearrangement also induces an increase in structural heterogeneity. Therefore, mechanical force-based destruction serves as the link between structure and function. Taken together, the structure in the dotted rectangle in Figure 3D suggests that local cellular remodeling weakens the collagen to the level that physiologically relevant mechanical forces eventually disrupt the alveolar wall, which, in turn, results in increased structural heterogeneity and decline in lung function.

In conclusion, we have found that structure–function relations exist in the lung undergoing heterogeneous changes after elastase injury as a model of emphysema. Furthermore, we have also shown that mechanical force–induced failure of the locally weakened collagen is a simple mechanism that simultaneously drives changes in both structure and function. With regard to the implications, one should recognize that the evaluation of any new animal model or novel treatment of emphysema, or, potentially, other diseases, could benefit from the detailed analysis of structure–function relations. Indeed, it is important to predict whether or not lung function would benefit from a small change in structure associated with a particular treatment (44). In addition to the structure–function relations, it is also important to identify various cellular and molecular processes that sustain inflammation and the secretion of enzymes in the parenchyma. Hence, molecular and structure–function studies should complement each other to bring this debilitating disease under control.

Author Disclosure: None of the authors has a financial relationship with a commercial entity that has an interest in the subject of this manuscript.

Acknowledgments: The authors thank Dr. Susumu Sato for helping with the isolated lung experiments, Robert Suki for the surfactant biochemistry, and Ashley Towner for the elastin–collagen staining.

References

1. Snider GL. Chronic obstructive pulmonary disease: a definition and implications of structural determinants of airflow obstruction for epidemiology. *Am Rev Respir Dis* 1989;140:S3–S8.
2. Lopez AD, Murray CC. The global burden of disease, 1990–2020. *Nat Med* 1998;4:1241–1243.
3. Barnes PJ, Stockley RA. COPD: current therapeutic interventions and future approaches. *Eur Respir J* 2005;25:1084–1106.
4. Janoff A. Elastases and emphysema: current assessment of the protease–antiprotease hypothesis. *Am Rev Respir Dis* 1985;132:417–433.
5. Barnes PJ. Chronic obstructive pulmonary disease. *N Engl J Med* 2000; 343:269–280.
6. Retamales I, Elliott WM, Meshi B, Coxson HO, Pare PD, Sciurba FC, Rogers RM, Hayashi S, Hogg JC. Amplification of inflammation in emphysema and its association with latent adenoviral infection. *Am J Respir Crit Care Med* 2001;164:469–473.
7. MacNee W. Oxidants/antioxidants and COPD. *Chest* 2000;117:303S–317S.
8. Demedts IK, Demoor T, Bracke KR, Joos GF, Brusselle GG. Role of apoptosis in the pathogenesis of copd and pulmonary emphysema. *Respir Res* 2006;7:53.
9. Finlay GA, O'Donnell MD, O'Connor CM, Hayes JP, FitzGerald MX. Elastin and collagen remodeling in emphysema: a scanning electron microscopy study. *Am J Pathol* 1996;149:1405–1415.

10. Vestbo J, Prescott E, Lange P. Association of chronic mucus hypersecretion with FEV_1 decline and chronic obstructive pulmonary disease morbidity. Copenhagen City Heart Study Group. *Am J Respir Crit Care Med* 1996;153:1530–1535.
11. Mishima M, Hirai T, Itoh H, Nakano Y, Sakai H, Muro S, Nishimura K, Oku Y, Chin K, Ohi M, *et al.* Complexity of terminal airspace geometry assessed by lung computed tomography in normal subjects and patients with chronic obstructive pulmonary disease. *Proc Natl Acad Sci USA* 1999;96:8829–8834.
12. Baldi S, Miniati M, Bellina CR, Battolla L, Catapano G, Begliomini E, Giustini D, Giuntini C. Relationship between extent of pulmonary emphysema by high-resolution computed tomography and lung elastic recoil in patients with chronic obstructive pulmonary disease. *Am J Respir Crit Care Med* 2001;164:585–589.
13. Bates JH, Davis GS, Majumdar A, Butnor KJ, Suki B. Linking parenchymal disease progression to changes in lung mechanical function by percolation. *Am J Respir Crit Care Med* 2007;176:617–623.
14. Suki B, Lutchen KR, Ingenito EP. On the progressive nature of emphysema: roles of proteases, inflammation, and mechanical forces. *Am J Respir Crit Care Med* 2003;168:516–521.
15. Lutchen KR, Yang K, Kaczka DW, Suki B. Optimal ventilation waveforms for estimating low-frequency respiratory impedance. *J Appl Physiol* 1993;75:478–488.
16. Ito S, Ingenito EP, Arold SP, Parameswaran H, Tgavalekos NT, Lutchen KR, Suki B. Tissue heterogeneity in the mouse lung: effects of elastase treatment. *J Appl Physiol* 2004;97:204–212.
17. Parameswaran H, Majumdar A, Ito S, Alencar AM, Suki B. Quantitative characterization of airspace enlargement in emphysema. *J Appl Physiol* 2006;100:186–193.
18. Kononov S, Brewer K, Sakai H, Cavalcante FS, Sabayanagam CR, Ingenito EP, Suki B. Roles of mechanical forces and collagen failure in the development of elastase-induced emphysema. *Am J Respir Crit Care Med* 2001;164:1920–1926.
19. Collins RA, Ikegami M, Korfhagen TR, Whitsett JA, Sly PD. *In vivo* measurements of changes in respiratory mechanics with age in mice deficient in surfactant protein D. *Pediatr Res* 2003;53:463–467.
20. Ito S, Ingenito EP, Brewer KK, Black LD, Parameswaran H, Lutchen KR, Suki B. Mechanics, nonlinearity, and failure strength of lung tissue in a mouse model of emphysema: possible role of collagen remodeling. *J Appl Physiol* 2005;98:503–511.
21. Lundblad LK, Thompson-Figueroa J, Leclair T, Sullivan MJ, Poynter ME, Irvin CG, Bates JH. Tumor necrosis factor–alpha overexpression in lung disease: a single cause behind a complex phenotype. *Am J Respir Crit Care Med* 2005;171:1363–1370.
22. Gardi C, Martorana PA, de Santi MM, van Even P, Lungarella G. A biochemical and morphological investigation of the early development of genetic emphysema in tight-skin mice. *Exp Mol Pathol* 1989; 50:398–410.
23. O'Donnell MD, O'Connor CM, FitzGerald MX, Lungarella G, Cavarra E, Martorana PA. Ultrastructure of lung elastin and collagen in mouse models of spontaneous emphysema. *Matrix Biol* 1999;18:357–360.
24. Ranga V, Kleinerman J. Lung injury and repair in the blotchy mouse: effects of nitrogen dioxide inhalation. *Am Rev Respir Dis* 1981;123: 90–97.
25. Shiomi T, Okada Y, Foronjy R, Schiltz J, Jaenish R, Krane S, D'Armiento J. Emphysematous changes are caused by degradation of type III collagen in transgenic mice expressing MMP-1. *Exp Lung Res* 2003;29:1–15.
26. Churg A, Dai J, Tai H, Xie C, Wright JL. Tumor necrosis factor–alpha is central to acute cigarette smoke–induced inflammation and connective tissue breakdown. *Am J Respir Crit Care Med* 2002;166:849–854.
27. de Santi MM, Martorana PA, Cavarra E, Lungarella G. Pallid mice with genetic emphysema: neutrophil elastase burden and elastin loss occur without alteration in the bronchoalveolar lavage cell population. *Lab Invest* 1995;73:40–47.
28. Foronjy RF, Okada Y, Cole R, D'Armiento J. Progressive adult-onset emphysema in transgenic mice expressing human MMP-1 in the lung. *Am J Physiol Lung Cell Mol Physiol* 2003;284:L727–L737.
29. Lucey EC, Goldstein RH, Stone PJ, Snider GL. Remodeling of alveolar walls after elastase treatment of hamsters: results of elastin and collagen mRNA *in situ* hybridization. *Am J Respir Crit Care Med* 1998;158:555–564.
30. Sly PD, Collins RA, Thamrin C, Turner DJ, Hantos Z. Volume dependence of airway and tissue impedances in mice. *J Appl Physiol* 2003;94:1460–1466.
31. Hantos Z, Adamicza A, Janosi TZ, Szabari MV, Tolnai J, Suki B. Lung volumes and respiratory mechanics in elastase-induced emphysema in mice. *J Appl Physiol* 2008;105:1864–1872.
32. Ito S, Bartolak-Suki E, Shipley JM, Parameswaran H, Majumdar A, Suki B. Early emphysema in the tight skin and pallid mice: roles of microfibril-associated glycoproteins, collagen, and mechanical forces. *Am J Respir Cell Mol Biol* 2006;34:688–694.
33. Kielty CM, Raghunath M, Siracusa LD, Sherratt MJ, Peters R, Shuttleworth CA, Jimenez SA. The tight skin mouse: demonstration of mutant fibrillin-1 production and assembly into abnormal microfibrils. *J Cell Biol* 1998;140:1159–1166.
34. Churg A, Wang RD, Tai H, Wang X, Xie C, Wright JL. Tumor necrosis factor-alpha drives 70% of cigarette smoke–induced emphysema in the mouse. *Am J Respir Crit Care Med* 2004;170:492–498.
35. Fisk DE, Kuhn C. Emphysema-like changes in the lungs of the blotchy mouse. *Am Rev Respir Dis* 1976;113:787–797.
36. Lappalainen U, Whitsett JA, Wert SE, Tichelaar JW, Bry K. Interleukin-1β causes pulmonary inflammation, emphysema, and airway remodeling in the adult murine lung. *Am J Respir Cell Mol Biol* 2005;32: 311–318.
37. Martorana PA, Brand T, Gardi C, van Even P, de Santi MM, Calzoni P, Marcolongo P, Lungarella G. The pallid mouse: a model of genetic alpha 1-antitrypsin deficiency. *Lab Invest* 1993;68:233–241.
38. Martorana PA, van Even P, Gardi C, Lungarella G. A 16-month study of the development of genetic emphysema in tight-skin mice. *Am Rev Respir Dis* 1989;139:226–232.
39. Ingenito EPTL, Majumdar M, Suki B. On the role of surface tension in the pathophysiology of emphysema. *Am J Respir Crit Care Med* 2005; 171:300–304.
40. Mouded M, Egea EE, Brown MJ, Hanlon SM, Houghton AM, Tsai LW, Ingenito EP, Shapiro SD. Epithelial cell apoptosis causes acute lung injury masquerading as emphysema. *Am J Respir Cell Mol Biol* 2009; 41:407–414.
41. Reiser K, McCormick RJ, Rucker RB. Enzymatic and nonenzymatic cross-linking of collagen and elastin. *FASEB J* 1992;6:2439–2449.
42. Vlahovic G, Russell ML, Mercer RR, Crapo JD. Cellular and connective tissue changes in alveolar septal walls in emphysema. *Am J Respir Crit Care Med* 1999;160:2086–2092.
43. Wilson TA, Bachofen H. A model for mechanical structure of the alveolar duct. *J Appl Physiol* 1982;52:1064–1070.
44. Suki B, Majumdar A, Nugent MA, Bates JH. *In silico* modeling of interstitial lung mechanics: implications for disease development and repair. *Drug Discov Today Dis Models* 2007;4:139–145.